Phases of deformation in filament networks with active cross-link slip

William McFadden, Edwin Munro

University of Chicago, Institute for Biophysical Dynamics, Chicago, IL 60615

(Dated: this day)

Abstract

Here we combine theoretical and computational approaches to explore mechanisms that govern long timescale deformation in semi-flexible filament networks with transient cross-links. We introduce a coarse-grained representation of cross-link dynamics in which cross-linked filaments slip past one another with an effective friction representing the time-averaged contributions of transient elastic cross-links. For small strains, we obtain a theoretical prediction for the long timescale effective viscosity of the network that depends on network architecture and effective friction coefficient between filaments, and we confirm this prediction using numerical simulations. We show computationally that network response deviates significantly from purely viscous creep when networks undergo large strains that drive them into anisotropic configurations. Interestingly, under certain conditions, we find a phase of long-lived sub-linear creep, suggesting that our simple model may account for the long-lived transitional phase between purely elastic and purely viscous rheology as measured in actin biopolymer experiments.

CONTENTS

I. INTRODUCTION

Cross-linked networks of semi-flexible polymers are a class of materials with poorly understood but highly interesting properties. Early studies of semi-flexible polymer networks

reconstituted *in vitro* revealed novel, nonlinear rheology, spurring interest from materials scientists[**?**]. Cross-linked networks of cytoskeletal polymers have been a subject of great interest to biologists because of their importance as structural components of cells[**?** **?**].

On shorter timescales, the response of cross-linked polymer networks to applied stress can be well-described theoretically in terms of purely elastic mechanical resistance. On longer timescales, the network's elastic resistance begins to give way to a viscous relaxation of stored stress, but the mechanisms that govern this viscous relaxation remain poorly understood. It is important to understand the mechanism behind this long timescale relaxation of cross-linked polymer networks both for understanding their novel material properties as well as understanding how this effect may govern physiologically important cellular processes[**?**].

For *in vitro* reconstitutions, this viscous relaxation is thought to result from transient unbinding and rebinding of intermolecular cross-links[**?** **?**]. However, there is still no clear understanding of how local relaxations of network connectivity would give rise to a global viscous relaxation. In our work, we wish to expand upon a well-established mechanical picture of cross-linked semi-flexible polymer networks to incorporate slippage of cross-links over longer timescales.

A. Short Timescale Mechanics of Cross-linked Actin Filament Networks

Early *in vitro* studies of cross-linked actin filament networks revealed strikingly different elastic behaviors compared to the already well-understood flexible polymer gels [**?**]. The complexity of these behaviors drove a surge in both experimental and theoretical studies of semi-flexible networks. For a comprehensive review of this field we recommend [**?**], but we will shortly repeat some important milestones here.

1. Theories of Semi-flexible Filament Networks

Diversity and discrepancy in observations led a drive toward systematic *in vitro* experimental explorations of the rheology of cross-linked semi-flexible polymer networks at short timescales. In studies with rigid irreversibly cross-linked networks, it was found that differences in network structure could lead to remarkably different elastic moduli, suggesting distinct phases of mechanical response [**?**]. These discoveries in turn begat theoretical work

on the basic implications of the semi-flexible nature of filaments on network mechanics.

Prior work on the basic physics of individual semi-flexible polymers [**?** **?**], and comprehensive theories of semi-flexible filament solutions, [**?**] laid a groundwork for theoretical considerations of cross-linked networks. Beginning with the so-called "mikado model" descriptions[**?** **?**], it was determined that there should exist a minimum rigidity percolation threshold, and that the connectivity of the network determined whether the mechanical response was dominated by non-affine bending or affine stretching of filaments. Continuing to more explicit theories[**?**], the mechanics of rigidly cross-linked networks were shown to be well-described in terms of purely elastic stretching of filaments between cross-linked points.

2. Incorporating Effects of Cross-link Compliance

Despite the success of the theory for rigid cross-links, early studies showed that surprising qualitative differences in mechanical response could be traced to differences in the chosen cross-linker[**?** **?**]. In addition, many studies using more compliant cross-linkers showed that cross-linker compliance could give rise to different nonlinear rheological properties on short timescales[**?** **?** **?** **?**]. Making matters even more complicated, ongoing research has begun to uncover added complexity from more highly complex issues such as filament bundling[**?** **?**]and the effects of active cross-linking by molecular motors[**?**].

While theorists have built a number of largely successful models that help characterize different aspects of the cross-link dominated response[**?** **?** **?**], the diversity of behaviors of these networks makes a precise yet general theory more difficult.

B. Long Timescale Stress Relaxation from Transient Cross-link Unbinding

At long timescales, the purely elastic behavior of cross-linked networks gives way to fluid-like stress relaxation. Additionally, fluid-like flows have been observed in a number of cellular processes[**?** **?** **?** **?** **?** **?**]. In *in vitro* studies, long timescale creep behaviors are thought to arise predominantly from the transient nature of filament binding for most biologically relevant cross-linkers[**?** **?** **?** **?**]. While the importance of cross-link dynamics in determining the mechanical response of semi-flexible polymer networks has been known for at least 20 years[**?**], there is still a gap in our understanding of how microscopic cross-link

unbinding relates to viscous flows.

1. *Models of Stress Relaxation with Transient Cross-links*

The dependence of network rheology on cross-link unbinding is an active subject of theoretical research[**?**].

Several theoretical methods have addressed cross-link binding and unbinding directly [**?** **?**] in analytical approaches that allowed well-constrained fits for specific cross-linkers. These theories have therefore focused conceptually at the level of the cross-linked filament and were extended analytically to macroscopic networks. In another approach, modelers have taken cross-links as extended springlike structures [**?**] that are able to bind and unbind in simulated filament networks. Finally, other more ambitious simulations have even sought to interrogate the effects of cross-link unbinding in combination with the more complex mechanics of filament bundles[**?** **?**].

Ultimately, the complexity of the many theoretical approaches that have been applied to this problem have made it difficult to distinguish what, if any, core physical mechanisms may be sufficient to explain the observed forms of stress relaxation. We believe that serious qualitative understanding can be generated by focusing on some of the common elements exhibited in the aforementioned literature.

2. *Novelty of Cross-link Slip Approach*

Here, we introduce a coarse-grained representation of filament cross-linking in which cross-linked filaments which are able to slide past each other as molecular bonds form and rupture, akin to coarse-grained models of molecular friction[**?** **?** **?**]. This drag-like coupling has been shown to be an adequate approximation in the case of ionic cross-linking of actin[**?** **?**], and can be found in the theoretical basis of force-velocity curves for myosin bound filaments[**?**]. We propose that it will form a suitable bulk approximation in the presence of super molecular cross-links as well.

Importantly, this simplification allows us to extend our single polymer models to dynamical systems of larger network models for direct comparison between theory and modeling results. This level of coarse graining will therefore make it easier to understand classes of

behavior for varying compositions of cross-linked filament networks. In addition, it allows us to compute a new class of numerical simulations efficiently, which gives us concrete predictions for behaviors in widely different networks with measurable dependencies on molecular details.

II. EXPLANATION OF MODEL

A. Composite Cross-link & Filament Representation

We consider individual filaments as chains of springs with relaxed length l_s. The orientations of neighboring springs are linearly coupled. Filaments can therefore be represented as a sequence of nodes with positions $\mathbf{x_i}$ and nearest neighbor interactions of the form

$$|F_{i,i+1}|_{\parallel} = -\mu \cdot \frac{|\mathbf{x_{i+1}} - \mathbf{x_i}| - l_s}{l_s} \tag{1}$$

$$|F_{i,i+2}|_{\perp} = -\frac{\kappa}{l_s^2} \cdot acos\left(\frac{\mathbf{x_{i+2}} - \mathbf{x_{i+1}}}{|\mathbf{x_{i+2}} - \mathbf{x_{i+1}}|} \cdot \frac{\mathbf{x_{i+1}} - \mathbf{x_i}}{|\mathbf{x_{i+1}} - \mathbf{x_i}|}\right) \tag{2}$$

where, μ represents an extensional modulus of a filament, and κ represents a bending modulus. This is essentially a discretized equivalent to a model of filaments with separable extensional and bending moduli as in [**?**]. We define the totally elastic force on a node as

$$\nabla \mathcal{H}_i = |F_{i,i+1}|_{\parallel} + |F_{i,i+2}|_{\perp} \tag{3}$$

Here, we take the extensional modulus as a composite quantities related to both filament and cross-linker compliance in a manner similar to a recently proposed effective medium theory[**?**]. In the limit of highly rigid cross-links and flexible filaments, our model reduces to the pure semi-flexible filament models of [**?** **?**]. In the opposite regime of nearly rigid filaments and highly flexible cross links, our method is still largely similar to the model of [**?**] in small strain regimes before any nonlinear cross link stiffening. However, in departure from those models, the magnitude of the force on interior cross-links in our model is still the same as those on the exterior. This is a simplification of the varying levels of strain that would actually be present in these cross-linkers as addressed in [**?**], but we choose to ignore the slight variation in favor of an approximated, global mean approach.

B. 2D Network Formation

We choose to focus our attention on 2D networks both for their tractability as well as their relevance in the quasi-2D cytoskeletal cortex of many eukaryotic cells[**?**]. In addition, recent developments in 2D *in vitro* systems[**? ?**], make 2D models all the more interesting as a renewed focus of study.

We follow a mikado model approach by initializing a minimal network of connected unstressed linear filaments in a rectangular 2D domain. We generate 2D networks of these semi-flexible filaments by laying down straight lines of length, L, with random position and orientation. We then assume that some fixed fraction of overlapping filaments become cross-linked (defined in II C) at their point of overlap.

Although real cytoskeletal networks may form with non-negligible anisotropy, we focus on isotropically initialized networks for simplicity. We define the density using the average distance between cross-links along a filament, l_c. A simple geometrical argument can then be used to derive the number of filaments filling a domain as a function of L and l_c[**?**]. Here, we use the approximation that the number of filaments needed to tile a rectangular domain of size $W \times H$ is $2WH/Ll_c$, and that the length density is therefore $1/l_c$.

In the absence of cross-link slip, we expect the network to form a connected solid with a well defined elastic modulus[**? ?**]. These networks are only well-connected when the ratio of filament length to intercross-link spacing, L/l_c, is greater than ~ 6. Near this percolation threshold, there are only locally connected domains, and discussions of global network properties becomes less reasonable. Additionally, as the filament density is increased beyond this point, there is another transition between non-affine bending and affine stretching of filaments, which changes the dominating term of the network's elastic modulus.

C. Drag-like Coupling Between Overlapping Filaments

In contrast to previous models, we allow relaxation of the network's stored stress by letting the attachment points slip. We do this by replacing an elastic interaction between pairs of points along filaments with a drag-like coupling between filaments.

$$\mathbf{F_{drag}} = \xi \cdot \int ds \, (\mathbf{v_i}(\mathbf{s}) - \mathbf{v_j}(\mathbf{s})) \, p_{ij}(s) \tag{4}$$

Where $p_{ij}(s)$ represents the locational distribution of cross-link points (equal to 1 at

locations of cross-links and 0 elsewhere) and $\mathbf{v_i}(\mathbf{s})$ and $\mathbf{v_j}(\mathbf{s})$ represent the the velocities of the ith and jth filaments. This model assumes a linear relation between applied force and the velocity difference between attached filaments. Obviously, non-linearities can arise in the presence of force dependent detachment kinetics as well as non-linear force extension of cross-links. We address non-linear effects of stress induced unbinding in Appendix A. Assuming inhomogeneities from non-linear effects are of second order, the motion for the entire network is governed by a dynamical equation of the form

$$\int ds \left(\zeta \mathbf{v_i}(\mathbf{s}) + \xi \sum_j (\mathbf{v_i}(\mathbf{s}) - \mathbf{v_j}(\mathbf{s}))\, p_{ij}(s)\right) = \nabla \mathcal{H}_i \tag{5}$$

Here, the first term in the integral is the filament's intrinsic drag through its embedding fluid, ζ, while the second comes from the drag-like coupling between filaments, ξ.

D. System of Equations for Applied Stress

We model our full network as a coupled system of differential equations satisfying 5. Although the general mechanical response of this system may be very complex, we focus our attention on low frequency deformations and the steady-state creep response of the system to an applied stress. To do this we introduce a fixed stress, σ along the midline of our domain. This stress points in the direction, $\hat{\mathbf{u}}$, producing either shear ($\hat{\mathbf{u}} = \hat{\mathbf{x}}$) or extensional ($\hat{\mathbf{u}} = \hat{\mathbf{y}}$) stress.

Finally, we add a 0 velocity constraint at the far edges of our domain of interest. We assume that our network is in the "dry," low Reynold's number limit, where inertial effects are so small that we can equate our total force to 0. Therefore, we have a dynamical system of wormlike chain filaments satisfying

$$\int ds \left(\zeta \mathbf{v_i}(\mathbf{s}) + \xi \sum_j (\mathbf{v_i}(\mathbf{s}) - \mathbf{v_j}(\mathbf{s}))\, p_{ij}(s)\right) = \nabla \mathcal{H}_i + \sigma \mathbf{u}(\hat{\mathbf{x}}) \tag{6}$$

subject to constraints such that $\mathbf{v_i}(\mathbf{x})$ is 0 with $x = 0$. This results in an implicit differential equation for filament segments which can be discretized and integrated in time to produce a solution for the motion of the system.

E. Computational Simulation Method

We tested our analytical conclusions on a computational model. More technical details of the model can be found in the Appendix, but we summarize the main modeling points here.

We discretize the filaments such that the equations of motion becomes a coupled system of equations for the velocities of filament endpoints, $\mathbf{x}$. The drag-like force between overlapping filaments results in a coupling of the velocities of endpoints.

$$\mathbf{A} \cdot \dot{\mathbf{x}} = \mathbf{f}(\mathbf{x}) \tag{7}$$

where $\mathbf{A}$ represents a coupling matrix between endpoints of filaments that overlap, and $\mathbf{f}(\mathbf{x})$ is the spring force between pairs of filament segment endpoints. We can then numerically integrate this system of equations to find the time evolution of the positions of all filament endpoints.

We generate a network by laying down filaments with random position and orientation within a domain of size $2D$ by D with periodic boundaries in the y-dimension. The external stress (shear or extensional/compressional) is applied to all filament endpoints falling within a fixed x-distance from the center of the domain. Finally, filament endpoints falling within a fixed x-distance from the edges of the domain are constrained to be nonmoving.

The nominal units for length, force, and time are μm, nN, and s, respectively. We explored parameter space around an estimate of biologically relevant parameter values, given in Table I.

TABLE I. Simulation Parameter Values

parameter	**symbol**	**physiological estimate**
extensional modulus	μ	$1nN$
bending modulus	κ	$10^{-3}nN \cdot \mu m$
cross-link drag coefficient	ξ	$unknown$
medium drag coefficient	ζ	$0.0005\frac{nNs}{\mu m^2}$
filament length	L	$5\mu m$
cross-link spacing	l_c	$0.5\mu m$
domain size	D	$10 - 50\mu m$

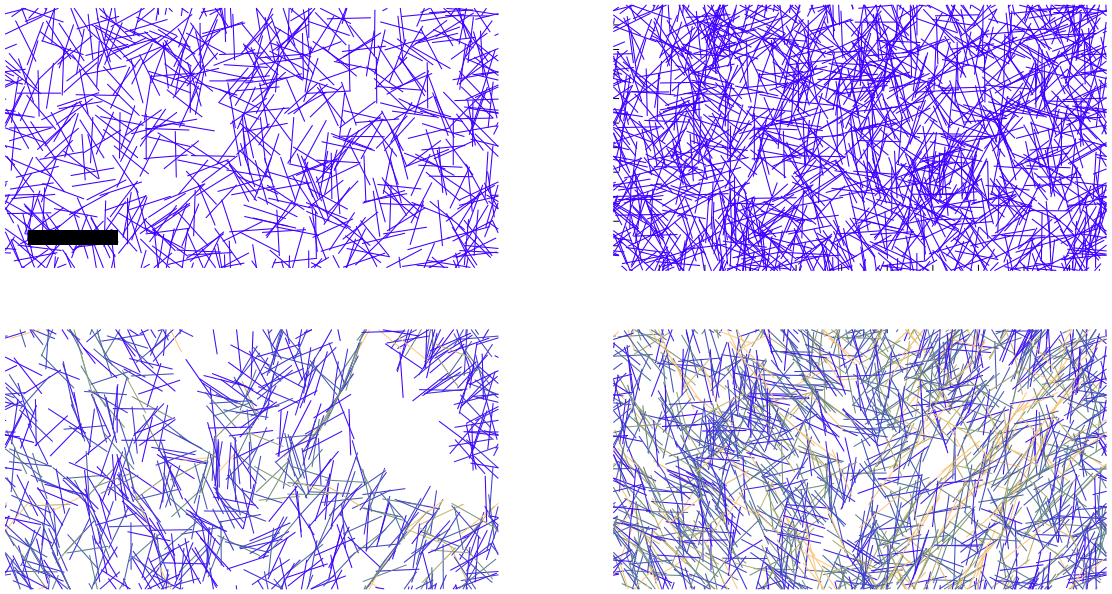

FIG. 1. Two Simulation setups with $L = 9\mu m, D = 54\mu m$ before (top) and after (bottom) 1000 seconds of applied stress. a) low density $l_c = 2\mu m$, b) moderate density $l_c = 1\mu m$. Scale bar $20\mu m$

For computational simplicity in these models, unless otherwise mentioned we assume that the bending rigidity, κ, is infinite. This allows us to model filaments as non-bending springs of rest length, L, and spring modulus μ. In the appendix, we show that our result is not significantly different from the result for semi-flexible polymers.

III. RESULTS

A. Steady-state Approximation of Effective Viscosity

We begin with a calculation of a strain rate estimate of the effective viscosity for a network described by our model in the limit of highly rigid filaments. We carry this out by assuming we have applied a constant stress along a transect of the network. With moderate stresses, we assume the network reaches a steady state affine creep. In this situation, we would find that the stress in the network exactly balances the sum of the drag-like forces from cross-link slip. So for any transect of length D, we have a force balance equation.

$$\sigma = \frac{1}{D} \sum_{filaments} \sum_{crosslinks} \xi \cdot (\mathbf{v_i}(\mathbf{x}) - \mathbf{v_j}(\mathbf{x})) \tag{8}$$

where $\mathbf{v_i}(\mathbf{x}) - \mathbf{v_j}(\mathbf{x})$ is the difference between the velocity of a filament, i, and the velocity of the filament, j, to which it is attached at the cross-link location, $\mathbf{x}$. We can convert the sum over cross-links to an integral over the length using the average density of cross-links, $1/l_c$ and invoking the assumption of (linear order) affine strain rate, $\mathbf{v_i}(\mathbf{x}) - \mathbf{v_j}(\mathbf{x}) = \dot{\gamma} x$. This results in

$$\sigma = \frac{1}{D} \sum_{filaments} \int_0^L \xi \cdot \left(\mathbf{v_i}(\mathbf{s}) - \mathbf{v_j}(\mathbf{s})\right) \frac{ds \cos\theta}{l_c}$$
$$= \sum_{filaments} \frac{\xi \dot{\gamma} L}{l_c} \cos\theta \cdot (x_l + \frac{L}{2} \cos\theta) \tag{9}$$

Here we have introduced the variables x_l, and θ to describe the leftmost endpoint and the angular orientation of a given filament respectively. Next, to perform the sum over all filaments we convert this to an integral over all orientations and endpoints that intersect our line of stress. We assume for simplicity that filament stretch and filament alignment are negligible in this low strain approximation. Therefore, the max distance for the leftmost endpoint is the length of a filament, L, and the maximum angle as a function of endpoint is $\arccos(x_l/L)$. The linear density of endpoints is the constant $D/l_c L$ so our integrals can be rewritten as this density over x_l and θ between our maximum and minimum allowed bounds.

$$\sigma = \frac{1}{D} \int_0^L dx_l \int_{-\arccos(\frac{x_l}{L})}^{\arccos(\frac{x_l}{L})} \frac{d\theta}{\pi} \frac{\xi \dot{\gamma} L}{l_c} \cdot \frac{D}{L l_c} \cdot (x_l \cos\theta + \frac{L}{2} cos^2\theta) \tag{10}$$

Carrying out the integrals and correcting for dangling filament ends leaves us with a relation between stress and strain rate.

$$\sigma = \frac{(L - 2l_c)^2 \xi}{4\pi l_c^2} \dot{\gamma} \tag{11}$$

We recognize the constant of proportionality between stress and strain rate as a viscosity. Therefore, our approximation for the effective viscosity, η_{eff}, at steady state creep in this low strain limit is

$$\eta_{eff} = \frac{(L - 2l_c)^2 \xi}{4\pi l_c^2}. \tag{12}$$

As illustrated in Figure 2, under moderate strains ($\gamma < 0.2$), our simulations show that in the high density limit, our theoretical approximation from Eqn 12 is highly accurate at explaining the network behavior. Aside from a geometrical factor, our approximation is valid for both shear and extensional stresses applied to the network.

As the density of the network approaches the breakdown limit, the effective viscosity diverges from our expected value. At the low connectivities, our expected viscosity goes to 0, but the medium viscosity begins to take over as we cross the percolation threshold at $L/l_c \sim 6$.

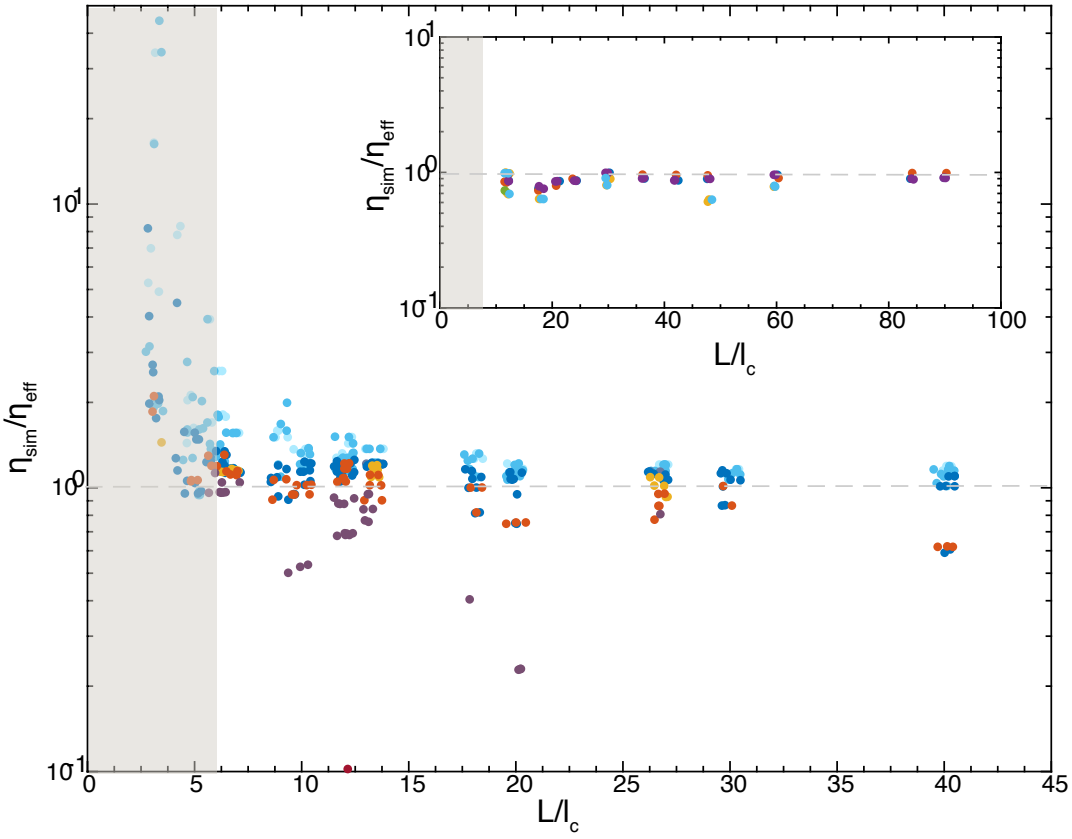

FIG. 2. Ratio of effective viscosity measured by shear simulation to predicted effective viscosity as a function of connectivity, L/l_c. Inset: Same measurement for extensional simulations

In addition to changing the architecture and effective drag coefficient, we also validated the generality of our approximation by varying simulation size, medium viscosity, filament stiffness, and applied stress. We were able to find a slight trend that depended on filament

stiffness as indicated in the difference between blue and red data points in Figure 2. The deviation from our approximation and variability in results manifested itself more strongly when filaments were highly compliant. To investigate this effect further, we next performed a more detailed analysis of the creep response while varying filament compliances.

B. Effects of Filament Compliance

The effect of filament compliance on cross-linked networks under strain is a subject of active research at the moment [Sayantan]. Therefore, we wished to use our computational approach to extend our understanding of filament networks in the regime of non-negligible filament compliance.

In irreversibly cross-linked polymer networks, filament compliance is known to give rise to elastic deformation of the network as described in[**?** **?**].

During the initial affine deformation immediately after the application of an external stress, we see a rapid stretch of filaments, $\langle \delta L/L \rangle_0$, in response to the affine purely mechanical strain, γ_{xy}, which closely follows $\langle \delta L/L \rangle_0 = \gamma_{xy} sin(\theta) cos(\theta)$. As shown in Figure 3, during the first phase in our simulations, the total network strain (solid) is described almost entirely by the strain of the filaments (dotted).

However, in the presence of cross-link slip, the filaments are not permanently constrained to remain at $\langle \delta L/L \rangle_0$. Interestingly, although the mean filament strain stays approximately constant, the distribution of individual filament strains broadens around the affine approximation as shown in the inset of Figure 3.

During the period where crosslink slip allows changes in the filament length distribution, we also find a long-lived intermediate relaxation phase that deviates from both the initial purely elastic relaxation and the later purely viscous behavior of section III A. In Panel B of Figure 3, we show that the standard deviation of the filament stretch distribution continues to increase throughout the period that the strain rate is non constant.

Approximating this broadening as a normally distributed variation in filament stretched length throughout the network ($\mathcal{N}$) with a time varying standard deviation, $\sigma(t)$, we have $\delta L/L = \langle \delta L/L \rangle_0 + \sigma(t) \cdot \mathcal{N}$. This has an effect on the total mechanical energy stored in the network $\mathcal{H} \sim \langle \delta L/L \rangle^2 = \langle \delta L/L \rangle_0^2 + \sigma(t)^2$. Therefore, the network will deform further while some strain energy is being stored in the further stretching filaments.

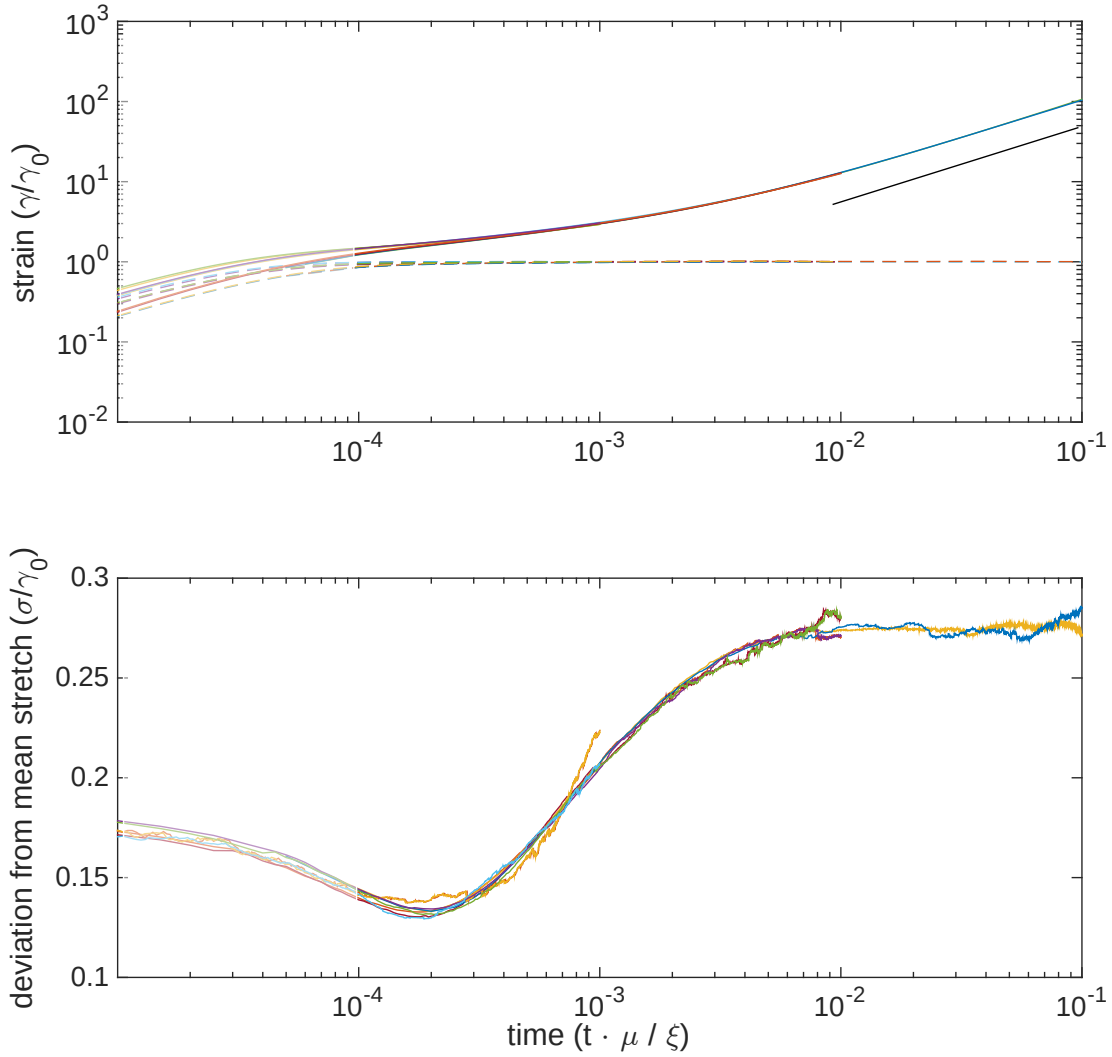

FIG. 3. Network and filament strain for different filament drag coefficient parameters. (top) Plot of total strain normalized by the final mean filament strain, $\delta L/L$. Dashed lines show the amount of strain from affine mechanical stretching. (bottom) Standard deviation of filament extension for the networks in A. Note that the creep compliance in A becomes constant (slope 1) only after the spread in filament extension in B stops increasing. Colors indicate unique experimental conditions.

Eventually the contribution from slow filament stretching will become negligible compared to that from pure cross-link slip on rigid rods. This occurs on a timescale similar to that of cross-link slip and causes the effective viscosity to decay back toward the rigid limit. This gives rise to a less-than-linear creep response during times after the initial elastic

relaxation but before full filament relaxation from cross-link slip. As shown in Figure 4, the transition begins to take place as network strain reaches 10 to 100 times the strain from pure mechanical stretching, $\gamma_0 = \delta L/L$, and this property is independent of the magnitude of the rate of strain.

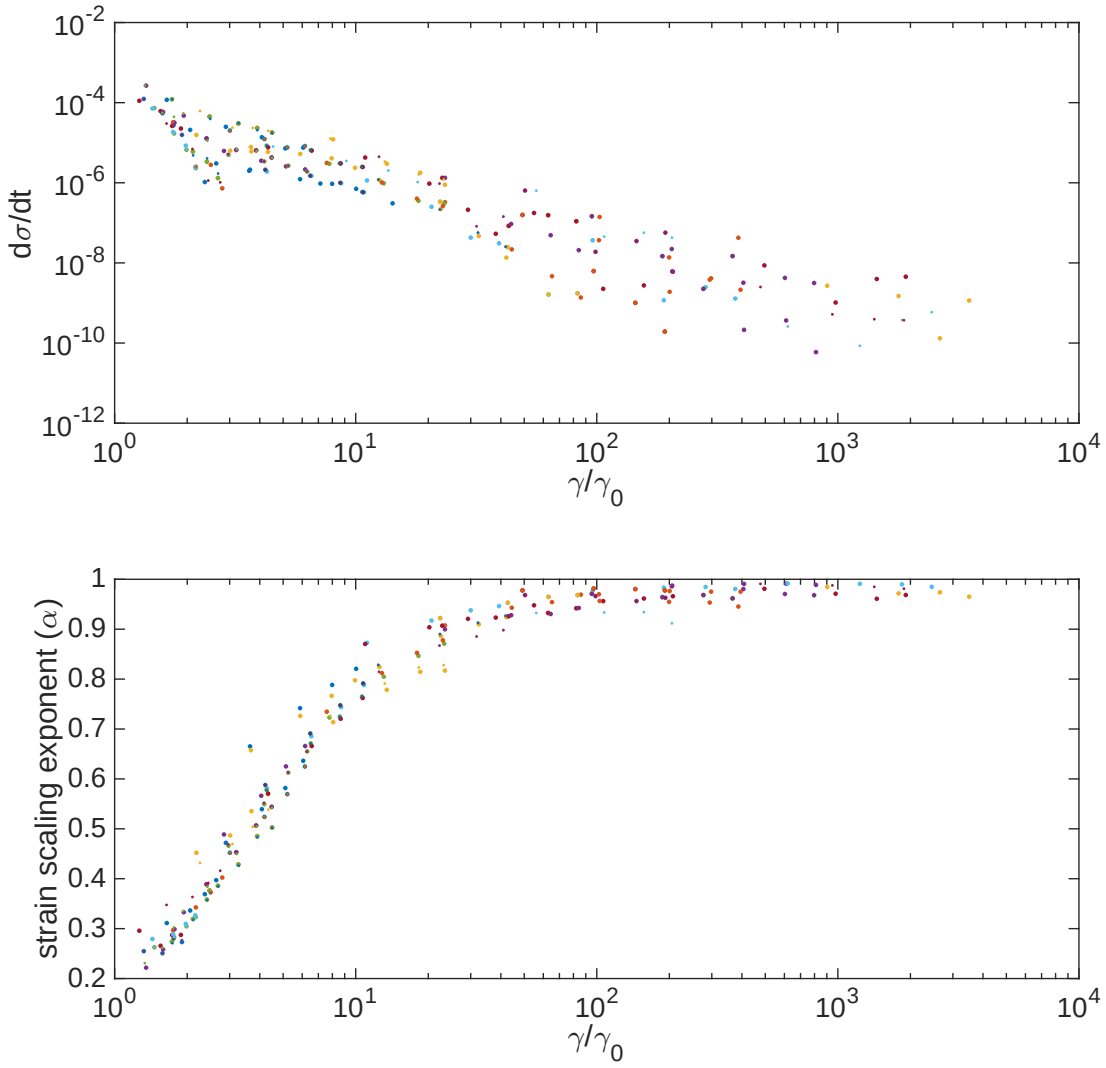

FIG. 4. Sublinear network strain ends as change in filament strain decays. (top) Change in standard deviation of filament strain, σ, as a function of strain relative to pure mechanical strain. (bottom) Dependence of strain rate exponent as a function of strain relative to pure mechanical strain, γ_0. Colors indicate unique experimental conditions.

C. Alignment at High Strain and Network Tearing

Once the network is able to accumulate a large strain, the assumption of nearly uniform distributions of filament orientations begins to break down.

At this point the filament orientations become unevenly distributed $\langle \delta L/L \rangle \neq \gamma_{xy} sin(\theta) cos(\theta)$, with a larger number of filaments aligning in the direction of extension rather than compression. Filament alignment, conceptually, causes the formation of subdomains that no longer span the space of the network. To the authors' knowledge an exact derivation of the dependence of network connectedness on filament alignment has not been carried out, but Monte Carlo simulations have been used to show that alignment does indeed lead to lower connectedness[**?**].

We find that over time, the orientational distribution of the filaments begins to peak around 45 degrees as the large strain induces alignment. In Figure 5, we see that as the angular standard deviation falls, this reorientation eventually leads to fewer bonds bridging the network perpendicular to the line of strain. As this connectivity begins to noticeably decrease, the observed effective viscosity decreases as well, giving rise to greater than linear creep. From the inset of Figure 5 we can also see that the onset of phase D occurred before the network had completely reached phase C, leading to a rapid transition between sub-linear and super-linear creep. Finally, it should be noted that the end of this simulation resulted in the network tearing apart.

D. Phase Diagram of Dominant Behavior

In Figure 6, we illustrate the four stereotyped phases of the general mechanical behavior that we observed in our networks. A deforming network typically undergoes a rapid filament stretching, a slower relaxation of elastic constraints, a phase of purely viscous cross-link slippage, and an eventual alignment and breakdown of network connectivity.

Finally, to explore the transitions between the various phases, we measured the creep response for a computationally tractable network ($L/l_c = 25$), as we varied the filament extensional modulus, μ, and the cross-link friction coefficient, ξ. In Figure 7, we classified parameter sets based on their strain exponent. We can see the trends for the transitions between phases A, B, and C. The line for the transition to D is still speculative at this time.

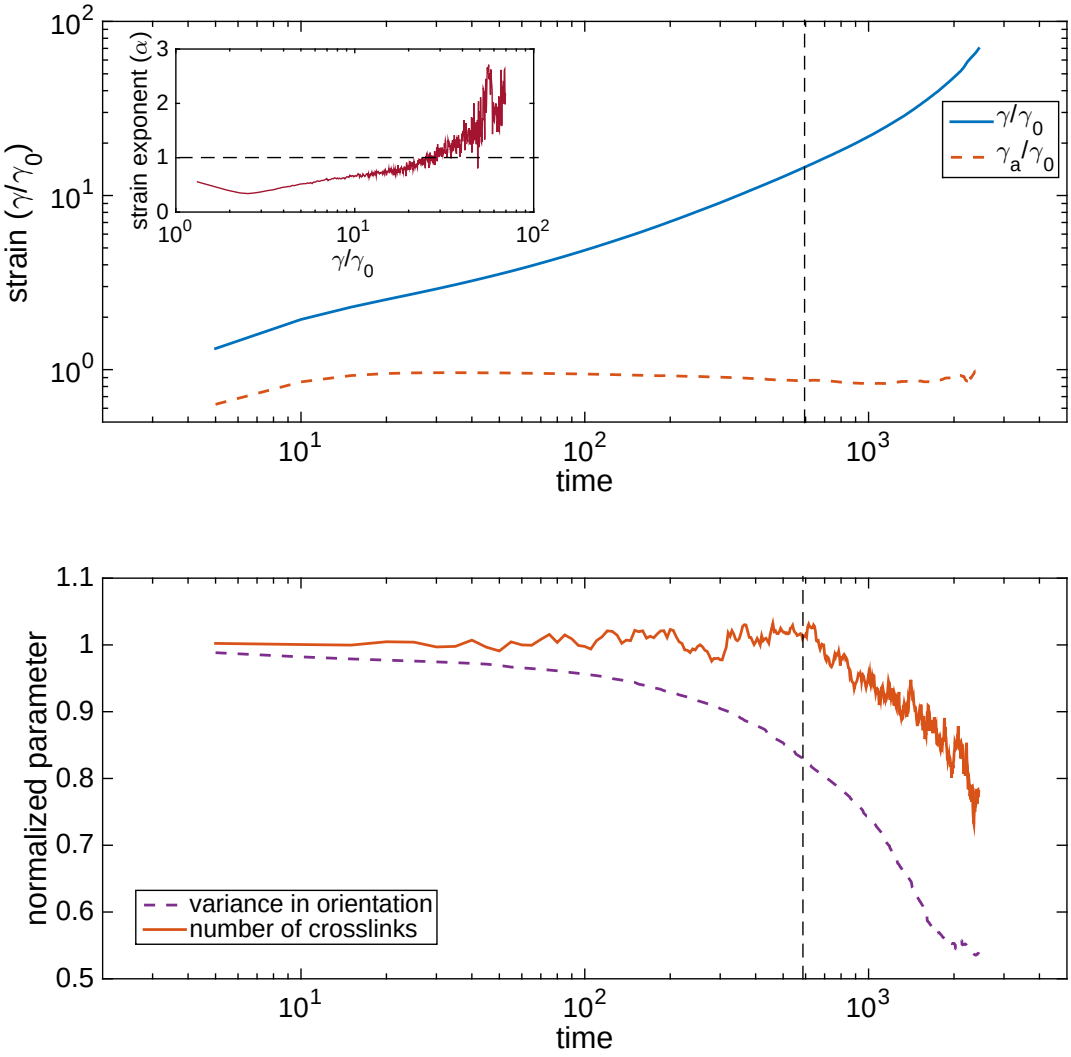

FIG. 5. Creep response of a network transitioning to phase D. (top) Strain curves for a network undergoing large scale deformation. Inset shows strain exponent as a function of strain (exponent passes 1). (bottom) Traces for the variance in filament orientation and number of cross links. Vertical dashed line shows the point where the strain exponent becomes greater than one.

IV. SUMMARY AND CONCLUSIONS

We have proposed a simplified effective friction model for understanding 2D cross-linked networks. Our model extends previous Mikado and lattice models to include effects of cross-link relaxation. We expect that our model can confer insights into mechanisms of network

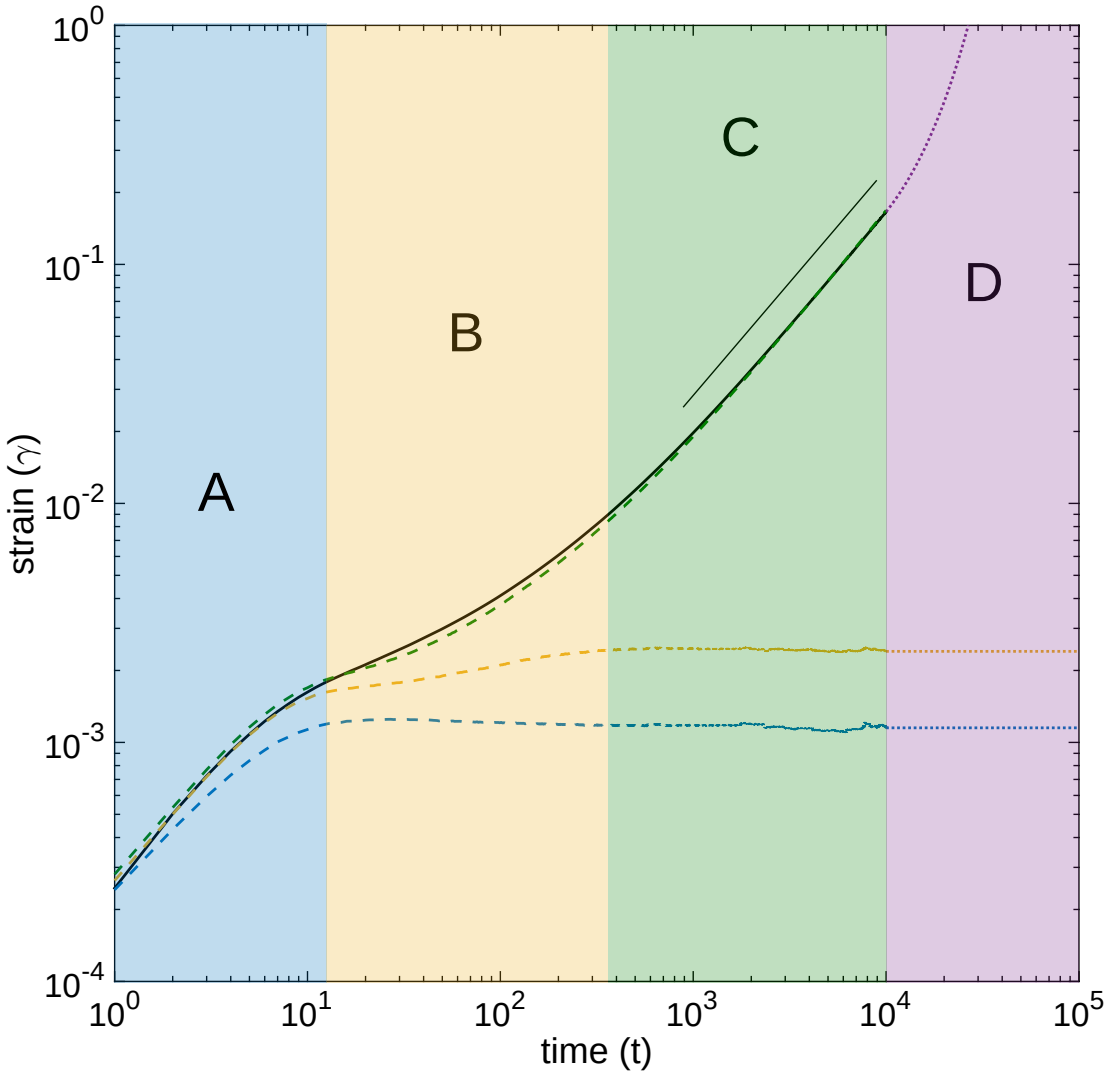

FIG. 6. Schematic of the general creep response of compliant filament networks illustrating the 4 phases of deformation: A) rapid mechanical response, B) combination of slow filament stretching and cross-link slip, C) cross-link slip dominated (line indicates slope of one), D) network tearing from filament alignment. Note that the portion of the curve in section D is only a hypothetical continuation of the actual data.

stress relaxation in quasi-2D networks such as those found in *in vitro* actin monolayer experiments[**?**] as well as in eukaryotic actomyosin cortices[**?**].

Our model is the first to address the plausible dependence of network effective viscosity on network structural properties. This led to a derivation of an estimate for the long

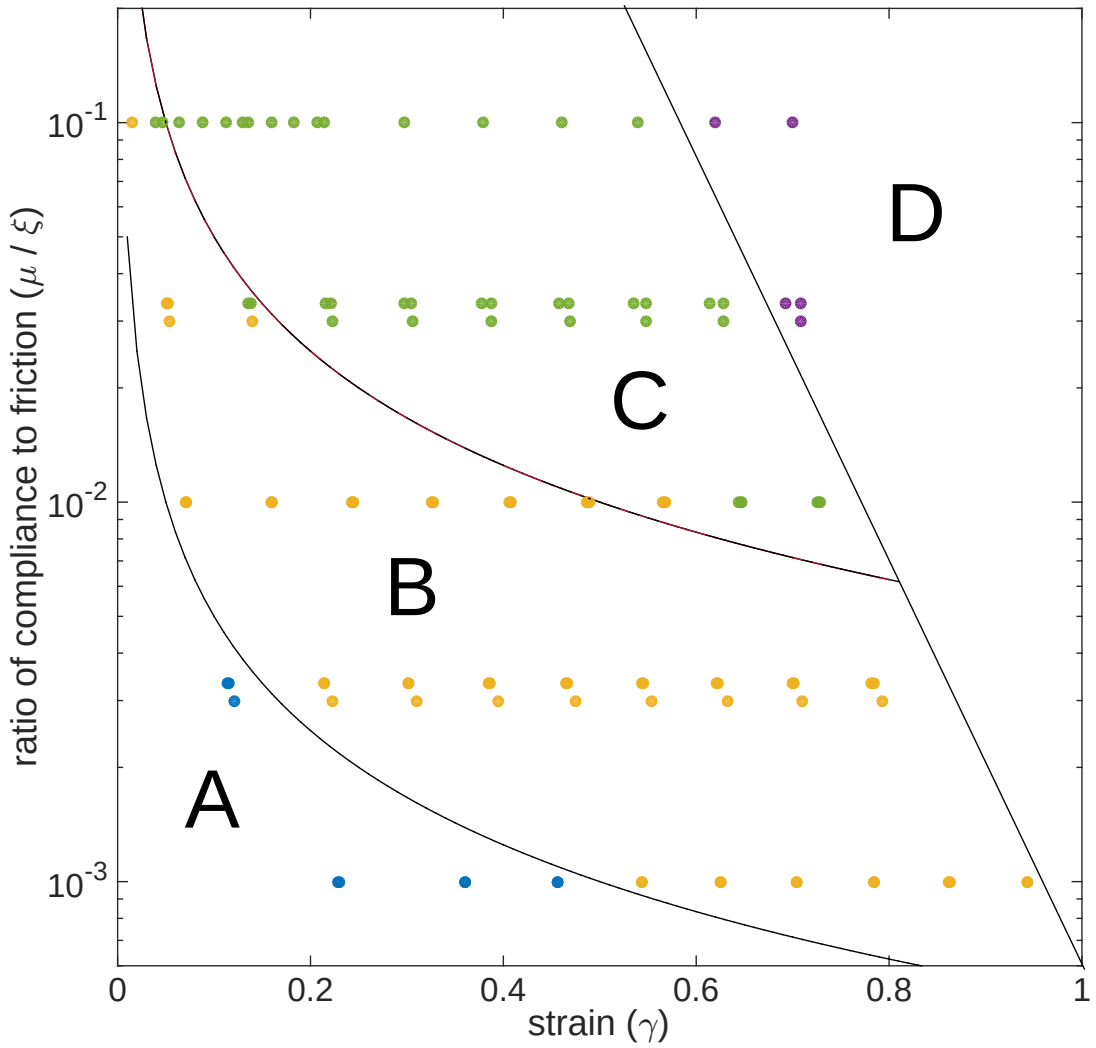

FIG. 7. phase diagram of creep response for different filament extension, μ and cross-link friction, ξ. Yellow, green, and purple dots correspond to creep measurements $\gamma \sim t^{\alpha}$ with $\alpha < 0.92$, $0.92 < \alpha < 0.98$, or $\alpha > 0.98$ respectively. Blue dots represent creep measurements where $\gamma_{total} < 2\gamma_{mechanical}$

timescale creep rate of networks under constant stress. Although this derivation neglects possible frequency dependence at short timescales, this finding offers a potential framework for addressing the dependence of network deformation rate on filament concentration and length.

Additionally, our simulations suggest that, in the presence of constant shear stress, cross-

link friction will also produce a long-lived phase of sublinear creep as filaments relax from their affine stretched position. While this phase may transiently resemble more explicit 3D models such as [**?**], it is clear that our model differs by predicting that network will achieve a constant effective viscosity more rapidly. In particular, we predict that this relaxation will occur at a rate similar to that of rate of cross-link slip derived strain and will therefore be negligible after the network has slipped by roughly ten times the magnitude of the purely affine mechanical deformation.

In building our model we have neglected any other sources of potential mechanical relaxation in order to simplify out analysis. In the future, we hope to extend our model to include biochemically driven forms of relaxation such as filament turnover or regulated cross-link unbinding.

This model forms a basis for addressing 2D filament network deformation, and it proposes a simplified formulation of important qualitative properties. In this way we are able to address potentially general phases of network deformation and delineate what network properties may give rise to them. This may provide an important starting point for addressing the general importance of network structure in more complex networks containing active elements.

V. ACKNOWLEDGEMENTS

I'd like to thank Shiladitya Banerjee and Sayantan Majumdar for discussions on this topic. Hopefully I can thank other people after I've spoken with them.

Appendix A: Deriving Molecular Drag Coefficients

Thus far, the idea of a molecular drag coefficient was taken as a phenomenological, measured parameter for a given experimental setup. While this is a sufficient pragmatic justification, it's useful to try to motivate the quantitative value of this drag coefficient by connecting it to the underlying cross-link properties of binding affinity, concentration, and extensibility.

To do this we'll imagine the simplified case of two cross linkers sliding past each other in one dimension. In this case, assume that we have an equilibrium number of bound cross-

linkers, n_B, each of which is displaced from its equilibrium length by some distance x. Each cross linker unbinds with rate k_{off} and rebinds at it's relaxed position ($x = 0$) with rate k_{on}. At the same time, all the cross linkers are being pulled from their relaxed position at a rate, v, which is simply the rate at which the filaments are sliding past each other.

We can write the differential equation for the change in the density of cross-links, ρ, at displacement x as they are pulled upon, bind, and unbind.

$$\frac{\partial \rho}{\partial t} = -k_{off}\rho(x) - v\frac{\partial \rho}{\partial x} + k_{on}\delta(x) \tag{A1}$$

Recognizing that $\int \rho(x) = n_B$ implies $k_{on} = k_{off}n_B$, we can find the steady state solution

$$\rho(x) = \frac{n_b k_{off}}{v} \cdot exp\left(-\frac{k_{off}}{v}x\right) \tag{A2}$$

If each cross-link has a spring constant μ_c, then we can equate the force on all cross-links to the applied force that is sliding the filaments past each other. Realistically, the spring constant and binding affinity would be functions of the cross-link stretch, but here we are taking them as approximately constant.

$$\int_0^\infty \rho(x)\mu_c x dx = v\frac{\mu_c n_B}{k_{off}} = F_{app} \tag{A3}$$

a

Therefore, the term next to v, (i.e. $\frac{\mu_c n_B}{k_{off}}$) would be equal to our molecular drag coefficient, ξ. Assuming approximately 1 cross link per filament overlap, and using parameter estimates culled from Ferrer et al., we build the following table of estimates for ξ.

cross-linker type	α-actinin	filamin-A
dissociation constant (s^{-1})	0.4	0.6
spring constant ($nN/\mu m$)	455	820
drag coefficient, ξ ($\frac{nN \cdot s}{\mu m}$)	182	492

This molecular description assumed both a constant off-rate and linear force extension of cross-links. In the event that binding kinetics are regulated by the state of extension, we would expect (based on Rf) to find a region that exhibits a stick-slip behavior instead of the smooth. Depending on the nature of any coupling between cross-links local stick-slip could either give rise to a global stick-slip behavior or a heterogenous mixture of stuck and

sliding cross-links. It would be interesting to explore this topic further in the future, but in the present analysis, we choose to ignore complications from these nonlinear effects.